Prediction of stability in boring using a multistep tool

Jaouher Selmi[1,3] · **Philippe Lorong**[2] · **Jean Philippe Costes**[1] · **Gérard Poulachon**[1] · **Patrice Carras**[3]

Received: 4 August 2015 / Accepted: 8 October 2015

Abstract This article presents an original study about the dynamic of a machining operation based on the coupling receptance methodology. The Frequency Response Function (FRF) of a machine tool is numerically coupled with the FRF matrix of a multi-stage reaming tool in order to predict its dynamic behavior during the operation. This coupling results in a mix of measured and numerical FRF matrix and is used for solving the stability prediction of the operation with an analytical methodology. Stability lobes are computed in respect with the load factor. It is shown in the paper that this methodology is suitable for adjusting the cutting conditions in the case of a given operation where the tool is identified but also for a numerical model of a tool, for instance at a design stage. As a conclusion, the presented methodology can help to target the best cutting conditions for a given machine-tool and toll but also help the manufacturer in the tool choice or design in order to guaranty the stability of the operation.

Keywords Chatter · Boring · Multistep tool · Stability

✉ Jaouher Selmi
jaouher.selmi@renault.com

Philippe Lorong
philippe.lorong@ensam.eu

Jean Philippe Costes
Jean-philippe.costes@ENSAM.eu

Gérard Poulachon
gerard.poulachon@ensam.eu

Patrice Carras
patrice.carras@renault.com

[1] Arts et Métiers ParisTech, LaBoMaP, Cluny, France

[2] Arts et Métiers ParisTech, PIMM, Paris, France

[3] Renault, DIPM, Guyancourt, France

NomenclatureMathematical notation

M	Matrix
$\overrightarrow{V}$	Vector
$\underline{q}$	Column

The parameters

K_t	Tangential cutting pressure
K_r	Radial cutting pressure
F_t	Tangential cutting force
F_r	Radial cutting force
f_z	Feed per tooth
b	Width of cut
h	Chip thickness
a_p	Depth of cut
V_c	Cutting speed
N	Rotation speed
K_r	Major tool cutting edge
Z	Insert number
Z^k	The insert number at the step k
$\overrightarrow{Q}$	Force screw (wrench)
$\overrightarrow{F}$	Force vector
$\overrightarrow{M}$	Moment vector
$\overrightarrow{D}$	Small displacement screw
$\overrightarrow{\theta}$	Rotation vector
$\overrightarrow{U}$	Lateral displacement vector
T	Time period between two teeth position
ω	Angular frequency
ω_c	Chatter angular frequency
Φ_j	Angular position of the tooth j
FRF	Frequency Response Function

1 Introduction

Besides machining-center power and torque limits, self-excited vibrations occurrence (chatter) constitutes a real

productivity limitation. Peklenik and Gartner [1], Pruvot [2], and Koppka [3] have shown that the stiffness lack in machining systems, strongly linked to chatter occurence, may have a negative effect on the produced workpiece accuracy. Hai Long [4] performed research on analyzing the chatter mechanism and suppression in the lathe process.

Tlusty [5] and Tobias [6] exposed the theory of regeneration; they demonstrated that the chatter instability is due to this phenomenon and appears when a depth of cut threshold is reached. Altintas and Budak [7] have set a model for stability chart prediction in the milling process. The stability lobe diagram is a chart which represents stability and instability domains during machining and allows the choice of preferential cutting conditions in order to increase the productivity and avoid vibration.

Altintas [8] and Budak [9] used an analytical method in frequency domain to predict stability chart in milling. Besides, Altintas [10] presented an analysis in discrete time domain to provide the stability chart in milling. Altintas [7] and Jochem [11] have also demonstrated the way to fit stability chart in the drilling process. When Bayly [12] considered that chatter is led by lateral vibration, Altintas [7] and Jochem [11] have considered also the axial and torsional d.o.f. (degree of freedom). They also noticed that the drilling and the boring process have the same dynamic behavior; this is why the same presented method can be extended to the boring process. In addition, Roukema [13] has performed a study using a time domain simulation to predict the stability of drilling operation regarding only axial and torsional degrees of freedom.

Otherwise, Selmi [14], Ertürk [15], Özsahin [16], and Albertelli [17] have performed studies on spindle and tool Frequency Response Function (FRF) prediction using receptance coupling. The dynamic model of the spindle linked to the dynamic model of the tool can give the FRF matrix at the tool tip. Having this input allows the stability prediction regarding the whole d.o.f. taken into account through the FRF matrix.

The present paper focus on the description of an extension of the stability method proposed in [8] to the boring process with a multistep tool (Section 2). The studied operation concerns a multistep tool with constant pitch. The cutting forces screw is expressed at the tool tip taking into account the insert repartition through the different steps. The FRF matrix at the tool tip is obtained by receptance coupling, representing the lateral translation and bending d.o.f.. Then, the dynamic equation of the boring operation is solved in the frequency domain, through an eigenvalue problem. A load factor is then introduced and makes the discrimination of stability suitable.

Experimental investigations are described in Section 3. They show how the model input can be obtained. Finally, in Section 4, an industrial application is presented and analyzed.

2 Dynamic model for the stability limits prediction

The proposed method is applied on a multistep tool containing (n) levels. This one is depicted on Fig. 1. For each step k, in a same way than for the beams theory, a cross section S_k is introduced. The cross section center of the step k is noted E_k. Thus, the center of the cross section at tool extremity is E_n. The radius r_k designates the radius at the step k.

The teeth number is supposed to be the same at the different tool steps.

The main used hypotheses are:

- The teeth belonging to a same step are supposed to have a rigid body motion.
- Moroever, the set of all steps of the tool are also supposed to have the same rigid body motion.
- The spindle and tool pair is supposed to get an axisymetric dynamic behavior. This one will be described at the tool extremity through the FRF matrix H. This matrix represents the dynamics of the rigid set of steps at E_n.
- The non-Galilean dynamic effect coming from the rotation of the tool are neglected and supposed to have no influence on the machining stability.

The main used coordinate systems are depicted on Figs. 2 and 3 and can be described as follows:

- $R_0\left(E_0, \overrightarrow{u_0}, \overrightarrow{v_0}, \overrightarrow{w_0}\right)$: The fixed coordinate system linked to the spindle housing. (E_0,w_0) is the theoretical rotating axis of the spindle.
- $R_e\left(E_0, \overrightarrow{u_e}, \overrightarrow{v_e}, \overrightarrow{w_0}\right)$: The rotating coordinate system following the motion of the spindle. The rotation position around the axis $\left(E_0, \overrightarrow{w_0}\right) = \left(E_0, \overrightarrow{w_e}\right)$ of the coordinate system is known through $\Phi_0=\Omega t$. The observation of the tool and the spindle deformation are done in this frame. These deformations remain small.
- $R_b\left(E_n, \overrightarrow{u_b}, \overrightarrow{v_b}, \overrightarrow{w_b}\right)$: The coordinate system attached to the rigid set of the steps of the tool. The motion of the steps are thus defined by the motion of R_b with respect to R_e. When the tool remains underformed, the coordinate systems R_e and R_b are superposed.
- $R_j^k : \left(p_j^k, \overrightarrow{u_J^k}, \overrightarrow{v_J^b}, \overrightarrow{w_J^k}\right)$: The coordinate system linked to the tooth (f) and the step k,$j \in \{0,1,2,\ldots,Z-1\}$.
- $R_j^{k,\text{local}} : \left(P_j^k, \overrightarrow{u_J^h}, \overrightarrow{v_J^b}, \overrightarrow{w_j^\Omega}\right)$: The local coordinate system of the tooth (j) and oriented by its cutting edge as shown in Fig. 3.

The two points E_0 and P_j^k are the origins of the tool and the j^{th} tooth coordinate system.

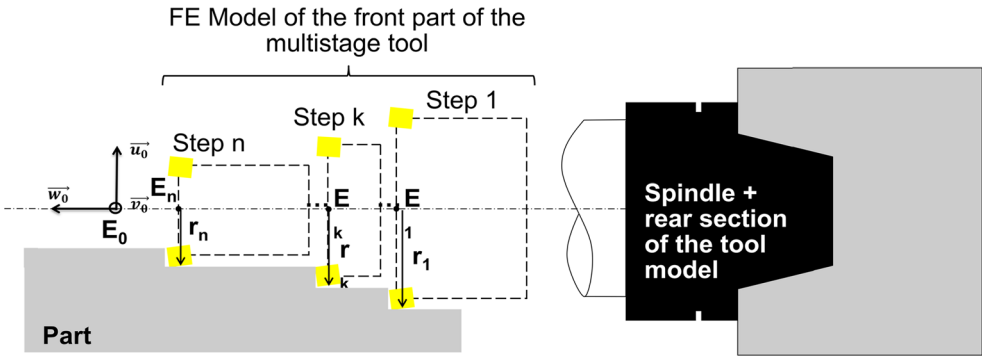

Fig. 1 Definition of a multistep tool

The regenerative motion of the tool is expressed in the rotating coordinate system R_e through a small displacement screw. This screw defines the motion of R_b with respect to R_e. It may be written at point E_n and any other point P_j^k belonging to the rigid set of steps. Then, it will be considered that $T = \frac{1}{z\Omega}$ is the time period separating two successive teeth. Knowing that all the steps have an equal teeth number, T is also the same for all steps.

2.1 Motion expression in R_e

Teeth motion with respect can be described thanks to a small displacement screw:

$$(D)(E_n) = \begin{pmatrix} \overrightarrow{\theta} \\ \overrightarrow{U}(E_n) \end{pmatrix} = \begin{pmatrix} \theta_u \overrightarrow{u_b} + \theta_v \overrightarrow{v_b} + \theta_w \overrightarrow{w_b} \\ u\overrightarrow{u_b} + v\overrightarrow{v_b} + w\overrightarrow{w_b} \end{pmatrix}, \quad (1)$$

where $\overrightarrow{\theta}$ and $\overrightarrow{U}$ are respectively the resultant (the rotation) and the moment (the displacement at E_n) of the small displacement screw.

$\underline{q}$ represents the d.o.f. column of the tool:

$$\underline{q} = \begin{pmatrix} \left(\overrightarrow{\theta}\right)_{R_b} \\ \left(\overrightarrow{U}(E_n)\right)_{R_b} \end{pmatrix}. \quad (2)$$

The column $\underline{q}$ contains six components: three for the rotation vector and three for the translation vector.

For the stability study, it will be considered that $\delta\underline{q} = \underline{q}(t) - \underline{q}(t-T)$. This formulation allows to deduce the position variation between the tooth (j) at (t) time and the tooth ($j+1$) at ($t-T$) time. Then:

$$(\delta D)(E_n) = \begin{pmatrix} \overrightarrow{\delta\theta} \\ \overrightarrow{\delta U}(E_n) \end{pmatrix} = \begin{pmatrix} d\theta_u \overrightarrow{u_b} + d\theta_v \overrightarrow{v_b} + d\theta_w \overrightarrow{w_b} \\ d\ u\overrightarrow{u_b} + d\ v\overrightarrow{v_b} + d\ w\overrightarrow{w_b} \end{pmatrix}. \quad (3)$$

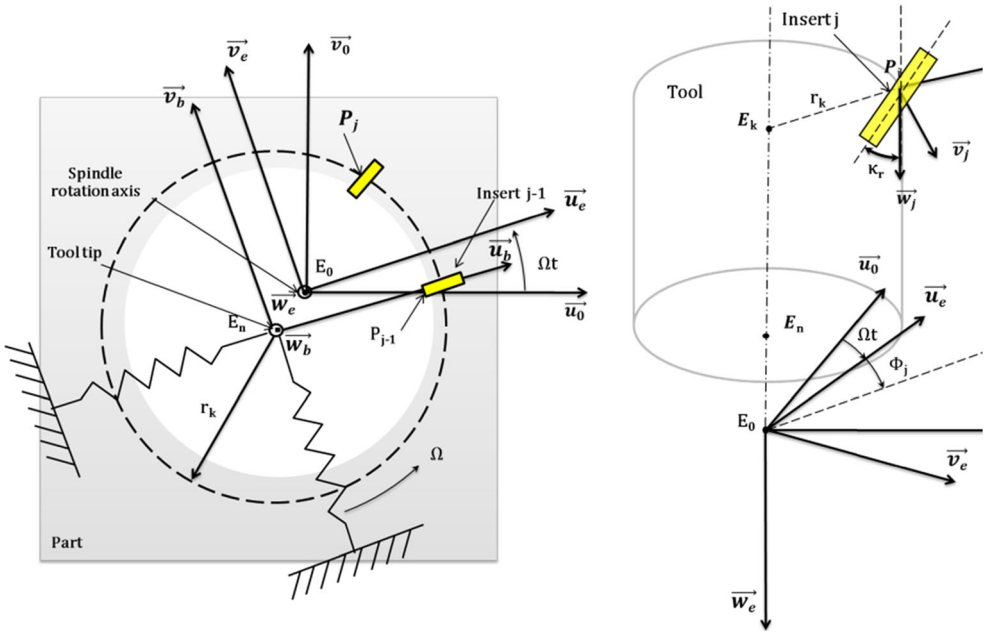

Fig. 2 Parametrizing of the boring operation

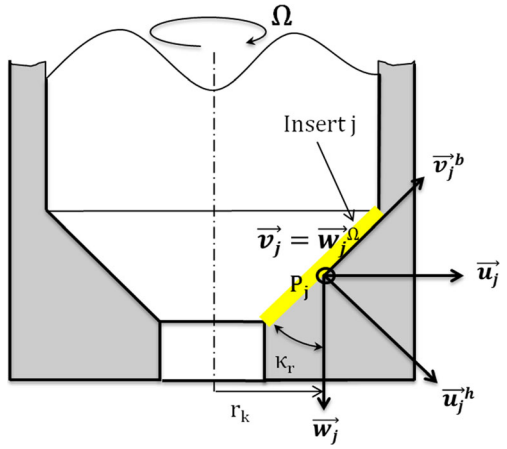

Fig. 3 Definition of the local basis for each insert (*j*)

2.2 The chip section

The aim of this paragraph is to express the variation of the chip thickness and chip width. These variations are due to the regenerative displacement of the tool.

The difference of position between the tooth (*j*) of the step (*k*) at (*t*) time and the tooth (*j*−1) at (*t*−*T*) time can be described through the vector $\overrightarrow{\delta s}_j^k$. This one contains the chip thickness δh_j^k and the chip width δb_j^k variations in the coordinate system $R_j^{k,\text{local}}$. The translation part of the small displacement screw can be expressed at the tooth (*j*) of the step (*k*) at P_j^k:

$$\overrightarrow{\delta U}\left(P_j^k\right) = \overrightarrow{\delta U}(E_n) + \overrightarrow{P_J^k E_n} \times \overrightarrow{\delta\theta}_{E_n'} \tag{4}$$

where $\left(\overrightarrow{P_J^k E_n}\right)$ is the vector defined in the coordinate system R_j^k as:

$$\left(\overrightarrow{P^k{}_J E}\right)_{R_j} = \begin{pmatrix} -r_j^k \\ 0 \\ w_j^k \end{pmatrix}. \tag{5}$$

$P_{R_j^k \to R_b}$ is the transfer matrix from the coordinate system R_j^k to R_b, defined as:

$$P_{R_j^k \to R_b} = \begin{pmatrix} c_j^k & -s_j^k & 0 \\ s_j^k & c_j^k & 0 \\ 0 & 0 & 1 \end{pmatrix} \quad \text{with} \quad \begin{matrix} c_j^k = \cos\left(\Phi_j^k\right) \\ s_j^k = \sin\left(\Phi_j^k\right) \end{matrix} \tag{6}$$

where

- $\Phi_j^k = j\Phi_p^k + \Phi_0^k$ is the angular position of the tooth *j*.
- $\Phi_p = \frac{2\pi}{z^k}$ is the angular pitch of the step *k*.
- Φ_0^k is the angular position of the tooth *j*=0, step *k*.

Thus, Eq. 4 can be expressed in R_b, the fixed reference as:

$$\left(\overrightarrow{\delta U}\left(P_j\right)\right)_{R_b} = \left(\overrightarrow{\delta U}(E_n)\right)_{R_b} + P_{R_j^k \to R_b}\left(\overrightarrow{P_j^k E_n}\right)_{R_j} \times \left(\overrightarrow{\delta\theta_{E_n}}\right)_{R_b}. \tag{7}$$

Then, the j^{th} tooth displacement at P_j^k is:

$$\left(\overrightarrow{\delta U}\left(P_j^k\right)\right)_{R_b} = \begin{pmatrix} du - r_j^k s_j^k d\theta_w - w_j^k d\theta_v \\ dv + r_j^k c_j^k d\theta_w + w_j^k d\theta_u \\ dw + r_j^k s_j^k d\theta_u - r_j^k c_j^k d\theta_v \end{pmatrix}. \tag{8}$$

The axial displacement (*dw*) at (P_j^k) is neglected compared to the transversal displacement. In addition, the tool torsion movement *dθ* is supposed to have no influence on the lateral vibration. Equation 8 became:

$$\left(\overrightarrow{\delta U}\left(P_j^k\right)\right)_{R_b} = M_j^k \underline{\delta q}$$

$$= \begin{pmatrix} 1 & 0 & 0 & 0 & -w_j^k & -r_j^k s_j^k \\ 0 & 1 & 0 & w_j^k & 0 & r_j^k c_j^k \\ 0 & 0 & 1 & r_j^k s_j^k & -r_j^k c_j^k & 0 \end{pmatrix} \begin{pmatrix} du \\ dv \\ dw \\ d\theta_u \\ d\theta_v \\ d\theta_w \end{pmatrix}. \tag{9}$$

The cutting section variation is represented by $\overrightarrow{\delta s_j^k}$ as:

$$\left(\overrightarrow{\delta s_j^k}\right)_{R_j^{k,\text{local}}} = \left(\overrightarrow{\delta U}\left(P_j^k\right)\right)_{R_j^{k,\text{local}}} = \begin{pmatrix} \delta h_j^k \\ \delta b_j^k \\ 0 \end{pmatrix}, \tag{10}$$

and

$$\overrightarrow{s_j^k} = \begin{pmatrix} \delta h_j^k \\ \delta b_j^k \end{pmatrix} = \begin{pmatrix} 1 & 0 & 0 \\ 0 & 1 & 0 \end{pmatrix} \left(\overrightarrow{\delta U}\right)_{R_j^{k,\text{local},}} \tag{11}$$

with

$$\begin{cases} \delta h_j^k = \overrightarrow{\delta U}_J\left(P_j^k\right).\overrightarrow{u}_j^h \\ \delta b_j^k = \overrightarrow{\delta U}_J\left(P_j^k\right).\overrightarrow{u}_j^b \end{cases}. \tag{12}$$

In order to express the relation between $\overrightarrow{\delta s_J}$ and $\delta\overrightarrow{U}\left(P_j\right)$, the transfer matrix $P_{R_j^k - R_j^{k,\text{local}}}$ from R_j^k to $R_j^{k,\text{local}}$ is introduced:

$$P_{R_j^k \to R_j^{k,\text{local}}} = \begin{pmatrix} c\kappa_j & 0 & s\kappa_j \\ s\kappa_j & 0 & -c\kappa_j \\ 0 & 1 & 0 \end{pmatrix} \quad \text{with} \quad \begin{matrix} c\kappa_j = \cos\left(\kappa_j\right) \\ s\kappa_j = \sin\left(\kappa_j\right) \end{matrix} \tag{13}$$

then,

$$\left(\overrightarrow{\delta s_J}\right)_{R_j^{k,\text{local}}} = \begin{pmatrix} \delta h_j^k \\ \delta b_j^k \\ 0 \end{pmatrix} = P_{R_j^k \to R_j^{k,\text{local}}}\left(P_{R_b \to R_j^k}\left(\delta\vec{U}\left(P_j^k\right)\right)_{R_b}\right). \quad (14)$$

Finally, Eqs. 9, 11, and 14 give $\underline{\delta s_j}$ as:

$$\underline{\delta s_j} = s_j^k \underline{\delta q}, \quad (15)$$

with

$$s_j^k = \begin{pmatrix} 1 & 0 & 0 \\ 0 & 1 & 0 \end{pmatrix} P_{R_j^k \to R_j^{k,\text{local}}} P_{R_b \to R_j^k} M_j^k. \quad (16)$$

2.2.1 The chip thickness

The chip thickness $h_j(t)$ of the tooth (j) at (t) can be written as:

$$h_j(t) = h_0 + \delta h_j(t), \quad (17)$$

where h_0 and $\delta h(t)$ are respectively the static and the dynamic chip thickness.

From the different teeth displacements determined in the previous section, the chip thickness can be deduced. It can be given by the projection of the displacement on $\overrightarrow{u}_j^h$:

$$\delta h_j = \left(\overrightarrow{\delta s_j}\right)_{R_j^{\text{local}}} \overrightarrow{u}_j^h. \quad (18)$$

The use of Eqs. 15, 16, and 18 gives:

$$\delta h_j = \begin{matrix} \langle c_j c\kappa_r & s_j c & \kappa_j & s\kappa_j \\ w_j s_j c\kappa_j + r_j s_j s\kappa_j & -w_j c_j c\kappa_j & -r_j c_j s\kappa_j & 0 \rangle \end{matrix} \begin{pmatrix} d\ u \\ d\ v \\ dw = 0 \\ d\ \theta_u \\ d\ \theta_v \\ d\ \theta_w \end{pmatrix}. \quad (19)$$

2.2.2 The chip width

As before, the cutting width variation is obtained by the displacement vector projection on the major tool cutting edge direction (Fig. 3).

$$\delta b_j = \left(\overrightarrow{\delta s_j}\right)_{R_j^{\text{local}}} \overrightarrow{v}_j^b. \quad (20)$$

Then,

$$\delta b_j = \begin{matrix} \langle c_j s\kappa_j & s_j s & \kappa_j & -c\kappa_j \\ w_j s_j s\kappa_j & -r_j s_j c\kappa_j & -w_j s_j c\kappa_j + r_j c_j c\kappa_j & 0 \rangle \end{matrix} \begin{pmatrix} d\ u \\ d\ v \\ dw = 0 \\ d\ \theta_u \\ d\ \theta_v \\ d\ \theta_w \end{pmatrix}. \quad (21)$$

2.3 Cutting forces

It is considered that cutting forces depend on the chip section. The force screw expressed at P_j^k is:

$$Q_j^k(\mathrm{h}, b)_{R_j^k} = Q_j^k(\mathrm{h}_0 + \delta\mathrm{h}, b_0 + \delta b) \quad (22)$$

where h_0,h,b_0, and b are the static and dynamic chip thickness, the static and dynamic chip width. The screw Q can be expressed as follows:

$$(Q)\left(P_j^k\right) = \begin{pmatrix} \overrightarrow{F}_j^k \\ \overrightarrow{M}_j^k\left(P_j^k\right) = \overrightarrow{0} \end{pmatrix}, \quad (23)$$

where $\overrightarrow{F}_j^k$ and $\overrightarrow{M}_j^k$ are the force and the moment applied on the tooth j. Depending on the chip section variation, the cutting force $\delta Q_j^k({h_{0,j}}^k, d\ {h_{0,j}}^k, {b_{0,j}}^k, d{b_{0,j}}^k)$ at the tooth (j) and the stage (k) can be expressed as:

$$\delta Q_j^k\left({h_{0,j}}^k, d{h_{0,j}}^k, {h_{0,j}}^k, d{h_{0,j}}^k\right) = Q_j^k\left(h_j^k, b_j^k\right) - Q_j^k\left({h_{0,j}}^k, {b_{0,j}}^k\right). \quad (24)$$

The force resultant part of the mechanical force screw can be expressed in $R_j^{\text{k,local}}$ as:

$$\underline{F_j^k} = \left(\overrightarrow{F_j}\right)^k_{R_j^{k,\text{local}}}. \quad (25)$$

For $\delta h_j^k \ll {h_{0,j}}^k$ *and* $\delta b_j^k \ll {b_{0,j}}^k$, a first order expansion leads to:

$$\underline{F_j^k}\left(h_j^k, b_j^k\right) \simeq \underline{F_j}\left({h_{0,j}}^k, {b_{0,j}}^k\right) + \nabla F_j\left({h_{0,j}}^k, {b_{0,j}}^k\right)\underline{\delta s_j^k}, \quad (26)$$

where ∇F_j^k is defined as:

$$\nabla F_j^k\left({h_{0,j}}^k, {b_{0,j}}^k\right) = \begin{pmatrix} \frac{\partial F_u}{\partial h} & \frac{\partial F_u}{\partial b} \\ \frac{\partial F_v}{\partial h} & \frac{\partial F_v}{\partial b} \\ \frac{\partial F_w}{\partial h} & \frac{\partial F_w}{\partial b} \end{pmatrix}_{\left({h_{0,j}}^k, {b_{0,j}}^k\right)}. \quad (27)$$

Equations 15 and 26 give:

$$\underline{F_j^k}\left(h_j{}^k, b_j{}^k\right) = \underline{F_j^k}\left(h_{0,j}{}^k, b_{0,j}{}^k\right) + \nabla \underline{F_j^k}\left(h_{0,j}{}^k, b_{0,j}{}^k\right) s_j^k \underline{\delta q}. \tag{28}$$

The dynamic part of the cutting force can be written as:

$$\underline{\delta F_j^k}(\mathrm{h}, b) = \nabla F_j^k\left(h_{0,j}{}^k, b_{0,j}{}^k\right) S_j^k \underline{\delta q}. \tag{29}$$

A second transfer matrix $P'_{R_j^k \to R_b}$ from the insert coordinate system R_j^k to R_b is introduced as:

$$P'_{R_j^k \to R_b} = \begin{pmatrix} P_{R_j^k \to R_b} & 0 \\ 0 & P_{R_j^k \to R_b} \end{pmatrix}. \tag{30}$$

The dynamic moment applied by the cutting force at the tool extremity E_n by the tooth j is expressed as follows:

$$\overrightarrow{\delta M}_j^k(E_n) = \overrightarrow{\delta M}_j^k\left(P_j^k\right) + \overrightarrow{E_n P_J} \times \overrightarrow{\delta F}\left(P_j^k\right), \tag{31}$$

where P_j^k, $\overrightarrow{\delta M}_j^k(E_n)$, $\overrightarrow{\delta M}_j^k\left(P_j^k\right)$, and $\overrightarrow{\delta F}\left(P_j^k\right)$ are respectively the center of the cutting edge of the tooth (j), the moment vector applied on (j) and expressed at E_n, the moment vector at P_j^k, and the force part applied at P_j^k.

Knowing that $\overrightarrow{M}_j^k\left(P_j^k\right) = \overline{0}$ (Eq. 23), Eq. 31 became:

$$\overrightarrow{\delta M}_j^k(E_n) = \overrightarrow{E_n P_j} \times \overrightarrow{\delta F}_j^{\mathrm{k}}\left(P_j^k\right). \tag{32}$$

In this context, the matrix O_j^k is introduced in order to sweeten the expression of the mechanical force screw at E_n. This matrix is defined as:

$$\begin{pmatrix} \left(\overrightarrow{\delta F}_j^{\mathrm{k}}\right)_{R_j^k} \\ \left(\overrightarrow{SM}_j^k(E_n)\right)_{R_j^k} \end{pmatrix} = O_j^{\mathrm{k}} \underline{\delta F_j} \quad \text{where} \quad O_j^k = \begin{pmatrix} 1 & 0 & 0 \\ 0 & 1 & 0 \\ 0 & 0 & 1 \\ 0 & -w & 0 \\ w & 0 & -r \\ 0 & r & 0 \end{pmatrix}. \tag{33}$$

As axial forces and torsion moments have no influence on lateral displacements, they will be neglected. Then, the matrix A is introduced in order to delete these components:

$$A = \begin{pmatrix} 1 & 0 & 0 & 0 & 0 & 0 \\ 0 & 1 & 0 & 0 & 0 & 0 \\ 0 & 0 & 0 & 1 & 0 & 0 \\ 0 & 0 & 0 & 0 & 1 & 0 \end{pmatrix}, \quad \text{with} \quad A \begin{pmatrix} F_u \\ F_v \\ F_w \\ M_u \\ M_v \\ M_w \end{pmatrix} = \begin{pmatrix} F_u \\ F_v \\ M_u \\ M_v \end{pmatrix}. \tag{34}$$

Then, the forces vector of the tooth (j), expressed at the spindle reference is as follows:

$$\underline{\delta Q_j^k} = A, P'_{R_j^k \to R_b}\left(\delta Q_j^k(\mathrm{h}, b)\right)_{R_j^k}. \tag{35}$$

The force contribution of the tooth j at the tool extremity En can be written as follows:

$$\underline{\delta Q_j^k} = A.P'_{R_j^k \to R_b \quad O_j^k P_{R_j^{k,\mathrm{local}} \to R_j}\left(\nabla F_j^k\right) S_j^k \underline{\delta q}}. \tag{36}$$

The addition of all the teeth force contribution gives the total dynamic forces applied on the tool, where:

$$\underline{\delta Q} = \sum_{k=1}^{n} \sum_{j=0}^{z-1} \underline{\delta Q_j^k} = \left\{ A \sum_{k=1}^{n} \sum_{j=0}^{z-1} P'_{R_j^k \to R_b} O_j^k P_{R_j^{k,\mathrm{local}} \to R_j}\left(\nabla F_j^k\right) S_j^k \right\} \underline{\delta q}. \tag{37}$$

The cutting force expression, as shown in Eq. 39, is general and can be applied for several cutting model. This equation will be used later with the dynamic equation of boring in order to study the stability of the operation. Such equation systems are complex to solve. The main used hypotheses are:

- The cutting force is proportional to the cutting area.
- The cutting force variation depends much more on the depth of cut variation than on the width of cut variation:

$$\frac{\partial F}{\partial h}(h_0, b_0) >> \frac{\partial F}{\partial b}(h_0, b_0).$$

Then,

$$\underline{\delta Q^k} = b_j^k \sum_{j=0}^{z-1} B_j^k(t) \underline{\delta q}, \tag{38}$$

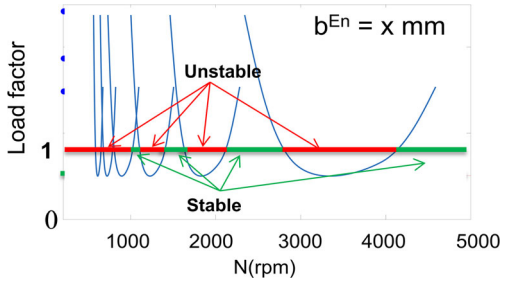

Fig. 4 The load factor diagram

with the matrix B_j is defined as:

$$B_j^k = \frac{1}{b_j^k} A.P'_{R_j^k \to R_b} O_j^k P_{R_j^{k,\text{local}} \to R_j} \left(\nabla F_j^k\right) S_j^k, \tag{39}$$

where Z and b^k are respectively the teeth number and the width of cut of the step (k). The matrix B_0^k is constant and can be deduced from Eq. 41:

$$B_0^k = \sum_{j=0}^{z-1} B_j^k = A \sum_{j=0}^{z-1} \left\{ \frac{1}{b_j^k} P_{R_j^k \to R_b} O_j P_{R_j^{k,\text{local}} \to R_j} \left(\nabla F_j^k\right) S_j^k \right\}. \tag{40}$$

Equations 38 and 40 give the total dynamic force vector per step (k):

$$\underline{\delta Q^k} = b^k B_0^k \underline{\delta q}. \tag{41}$$

Equation 38 became:

$$\underline{\delta Q} = \sum_{j=0}^{z^1-1} b^1 B_j^1 \underline{\delta q} + \ldots + \sum_{j=0}^{z^k-1} b^k B_j^k \underline{\delta q} + \ldots + \sum_{j=0}^{z^n-1} b^n B_j^n \underline{\delta q}. \tag{42}$$

Finally, Eq. 42 became:

$$\underline{\delta Q} = \left(b^1 B_0^1 + \ldots + b^k B_0^k + \ldots + b^n B_0^n\right) \underline{\delta q}. \tag{43}$$

2.4 Stability analysis model

An analytical approach for solving the multistep tool dynamic behavior equation is presented in this paragraph. For all steps, the depth of cut is constant and depends on the tool geometry. The presented approach shows how to evaluate the stability through the "load factor." This one will be presented later with more details.

The FRF matrix at the contact zone between the tool extremity E_n and the workpiece can be expressed as:

$$H = \begin{pmatrix} h_{uu} & 0 & h_{u\theta_u} & 0 \\ 0 & h_{vv} & 0 & h_{v\theta_v} \\ h_{u\theta_u} & 0 & h_{\theta_u\theta_u} & 0 \\ 0 & h_{v\theta_v} & 0 & h_{\theta_v\theta_v} \end{pmatrix}, \tag{44}$$

with

$$H\underline{Q} = \underline{q}. \tag{45}$$

The columns $\underline{Q}$ and $\underline{q}$ contain the forces/moments and the displacements/rotations expressed in R_e respectively at the tool extremity E_n.

The displacement vectors are defined between the times $(t-T)$ and (t) as:

$$\underline{q} = \begin{pmatrix} u(t) \\ v(t) \\ \theta_u(t) \\ \theta_v(t) \end{pmatrix}, \tag{46}$$

and

$$\underline{q_0} = \begin{pmatrix} u(t-T) \\ v(t-T) \\ \theta_u(t-T) \\ \theta_v(t-T) \end{pmatrix}. \tag{47}$$

The use of a harmonic function helps on describing vibrations at the frequency domain at the chatter frequency ω_c:

$$\underline{q}(i\omega_c) = H(i\omega_c t), \tag{48}$$

$$\underline{q_0}(i\omega_c) = e^{-i\omega_c T} \underline{q_0}(i\omega_c). \tag{49}$$

The displacement variation between the times (t) and $(t-T)$ can be described as follows:

$$\delta\underline{q}(i\omega_c) = \underline{q}(i\omega_c) - \underline{q_0}(i\omega_c). \tag{50}$$

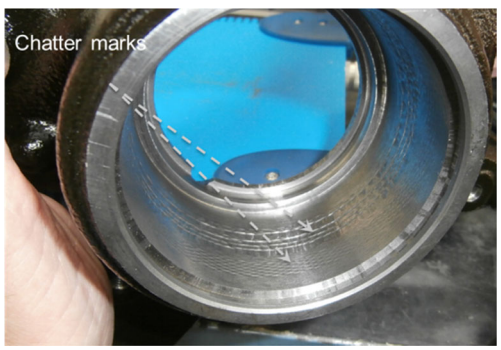

Fig. 5 Observation of the chatter marks

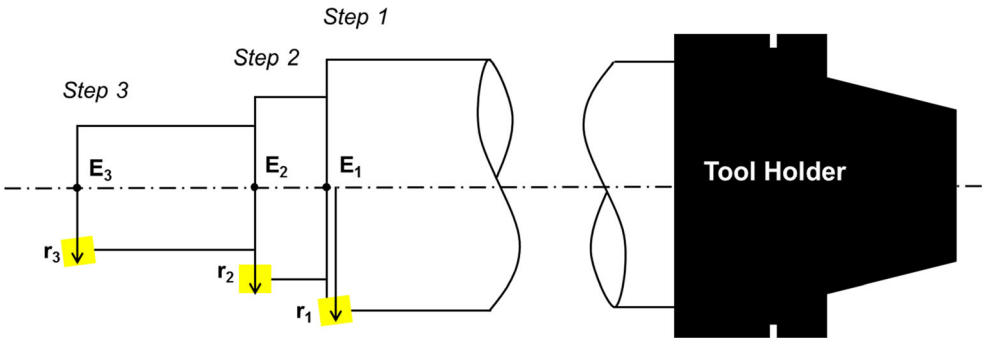

Fig. 6 The definition of the used tool

The substitution of Eqs. 48 and 49 into 50 gives:

$$\delta \underline{q}(i\omega_c) = \left(1-e^{-i\omega_c T}\right) H \delta \underline{Q}(i\omega_c T), \tag{51}$$

where $\omega_c T$ is the delay shift between two successive teeth. The substitution of $\delta q(i\omega_c)$ into Eq. 45 gives:

$$\delta \underline{Q} = \left\{b^1 B_0^1 + \ldots + b^k B_0^k + \ldots + b^n B_0^n\right\}\left(1-e^{i\omega_c T}\right) H \delta \underline{Q} e^{i\omega_c T}. \tag{52}$$

Equation 54 has a non-trivial solution if:

$$\det\left\{I-\left(b^1 B_0^1 + \ldots + b^k B_0^k + \ldots + b^n B_0^n\right)\left(1-e^{-i\omega_c T}\right) H\right\} = 0. \tag{53}$$

Equation 53 can be considered as an eigenvalue problem with:

$$\det(A + \lambda B) = 0, \tag{54}$$

where λ, A, and B are respectively the eigenvalues and the matrices. By identification, the next equations are obtained:

$$A = I, \tag{55}$$

$$B = \left(b^1 B_0^1 + \ldots + b^k B_0^k + \ldots + b^n B_0^n\right) H, \tag{56}$$

and

$$\lambda = \eta\left(1-e^{-\omega T)}\right). \tag{57}$$

The scalar η is the introduced "load factor" for the operation stability analysis. This factor is a real quantity and can be determined for one known width of cut b^{η}. If this factor is greater than 1, the operation can be considered stable. In the other case, the operation is unstable.λ is a complex quantity:

$$\lambda = \lambda_R + i\lambda_I. \tag{58}$$

Then,

$$e^{i\omega_c T} = \cos(\omega_c T) + i\ \sin(\omega_c T). \tag{59}$$

The substitution of Eqs. 61, 60, into 59 gives:

$$\lambda_R + i\lambda_I = -\eta(1-\cos(\omega_c T) - i\ \sin(\omega_c T)). \tag{60}$$

This leads finally to:

$$\eta = -\frac{\lambda_R(1-\cos(\omega_c T)) + \lambda_I \sin(\omega_c T)}{2(1-\cos(\omega_c T))} + i\frac{\lambda_I(1-\cos(\omega_c T)) - \lambda_R \sin(\omega_c T))}{2(1-\cos(\omega_c T))}. \tag{61}$$

Knowing that η is a real quantity, the imaginary part of Eq. 63 is equal to 0. Therefore,

$$\lambda_i(1-\cos(\omega_c T)) - \lambda_R \sin(\omega_c T) = 0. \tag{62}$$

κ is introduced as:

$$\kappa = \frac{\lambda_i}{\lambda_R} = \frac{\sin(\omega_c T))}{(1-\cos(\omega_c T))}. \tag{63}$$

The substitution of Eq. 63 into 61 gives the load factor expression as follows:

$$\eta = -\frac{\lambda_R}{2}\left(1+\kappa^2\right). \tag{64}$$

Then, the operation stability evaluation can be made for all chatter frequencies ω_c.

For the load factor diagram (N(RPM),n) establishment, the relation between the eigenvalues and the rotation speed should be demonstrated.

Table 1 Specifications of the tool steps

	Major tool cutting edge κ_r	Tool radius r_k	Maximal depth of cut
Step 1	85°	35.8 mm	1.9 mm
Step 2	90°	33.9 mm	2 mm
Step 3	85°	31.9 mm	5.1 mm

Knowing that the imaginary part of Eq. 63 is equal to 0, the angle ψ of λ can be expressed as:

$$\tan(\psi) = \kappa = \frac{\cos(\omega_c T/2)}{\sin(\omega_c T/2)} = \tan(\pi/2 - \omega_c T/2) \cdot \quad (65)$$

Then,

$$\psi = \tan^{-1}(\kappa) \cdot \quad (66)$$

In addition $\varepsilon = \pi - 2\psi$ is the delay between two modulations. For k integer, this delay can be expressed as:

$$\omega_c T = \varepsilon + 2k\pi \cdot \quad (67)$$

Then, the rotation speed expression is:

$$N = \frac{60}{ZT} = \frac{60\omega_c}{Z(\varepsilon + 2k\pi)} \cdot \quad (68)$$

2.5 The load factor diagram

The load factor diagram evaluates the stability of the boring multistep operation, for a known width of cut associated to the different steps. As for the stability lobe diagram, the diagram (Fig. 4) represents lobes separating two main domains: stable and unstable. The stable domain is situated under the lobes; however, the unstable domain is on the other side.

For the multistep tool, except for the last step where the depth of cut may vary, the different widths of cut of the other steps are determined by the tool geometry. The diagram shown on Fig. 4 is designed for one known depth of cut of the last step.

When the load factor take the value 1, the values on the stability lobe diagram correspond to the chosen cutting conditions. When this value is under the lobes, this means that the operation is stable (green line). In the other case, the operation is not stable (red line).

3 Experimental investigations

3.1 Context

The poor design of the machining structure can lead to many surface quality defects as can be shown in Fig. 5. The stripes depicted on the workpiece are the result of the instability of the cutting operation.

This experimental method section should allow the identification of the parameters which will be used as input for the analytical model for the stability prediction.

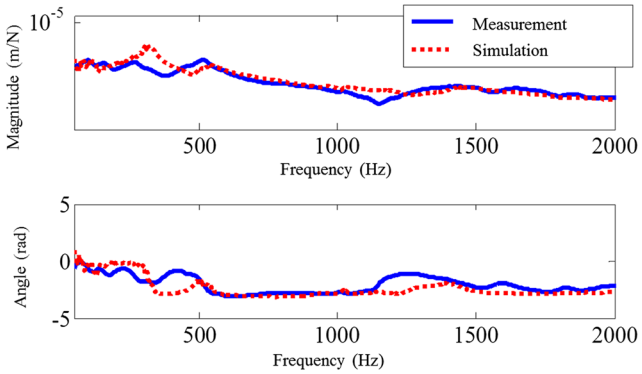

Fig. 7 The FRF at the tool tip achieved by measurement and simulation

3.1.1 The multistep tool

Figure 6 depicts the multistep tool containing nine inserts, evenly distributed on three steps. All of the inserts have the same cutting edge sharpness and the same corner radius r_ε equal to 1.2 mm.

Table 1 shows the multistep tool parameters and the different depth of cut taken by the different steps.

3.1.2 Cutting parameters

In the studied operation the main cutting conditions are:

- The revolution speed of the spindle: N=750 RPM
- The feed rate: V_f=350 mm/min (*or* f_z=0,15 mm/tooth).

3.2 The FRF matrix at the tool extremity

The knowledge of the FRF at the tool extremity is of interest for the stability study. A unique lateral hammer test is not enough to get all the components of the FRF matrix at tool extremity. All the components of the transfer matrix are necessary to supply the input of the stability predictive analytical model, even those corresponding to the bending d.o.f..

This is why this matrix was obtained through the coupling receptance methodology described by Selmi [14] and Albertelli [17] which allows the obtention of the FRF matrix for all the degrees of freedom. In this way, the machine tool

Table 2 The identified Kienzle parameters

Tool	Cutting force component	κ_i	m_i
κ_r=90	F_t	1264	0,27
κ_r=90	F_r	691	0,17
κ_r=85	F_t	1320	0,21
κ_r=85	F_r	235	0,63

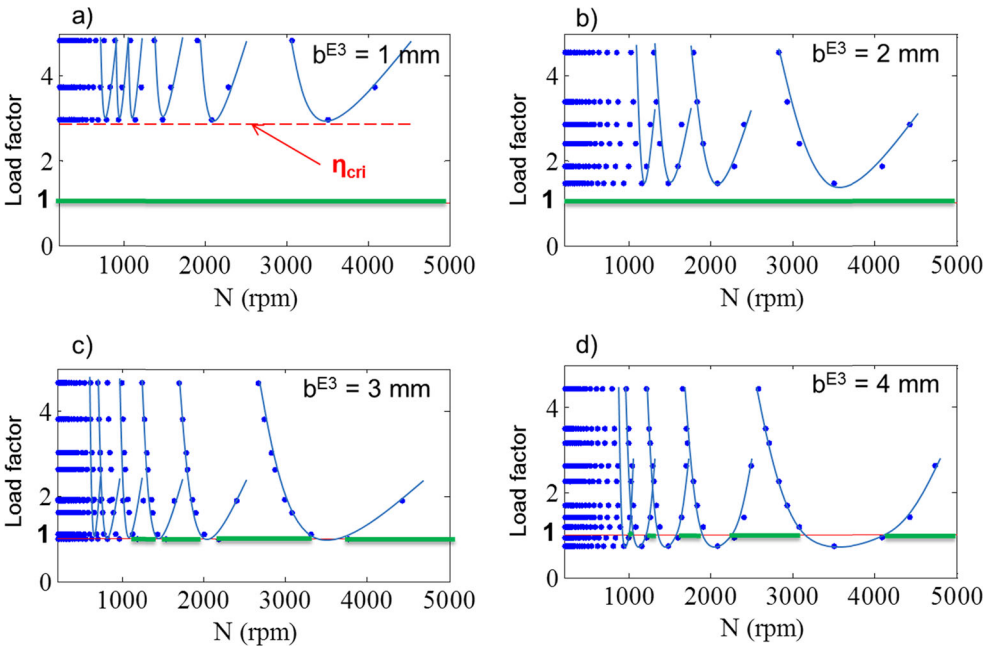

Fig. 8 The stability evolution for the multistep tool

FRF matrix was identified and coupled with the FRF matrix of the FE model of the tool.

Then, the lateral component of the FRF calculated matrix was compared with an experimental lateral FRF obtained by hammer test as noticed in Fig. 7. Small differences are seen and due to the FE model of the tool.

3.3 Cutting parameters identification

A cutting forces measurement is conducted using a CNC lathe SONIM T9 with a 30 kW spindle power. Two tools, with different major tool cutting edge 85° and 90° are used.

Here, the Kienzle model was chosen because of its good correlation and representativity for several measurements by identifying only two factors for each component. The expression of the Kienzle [18] cutting force model is:

$$F_i = K_i b h^{1-m_i} \tag{69}$$

The coefficient K_i and the exponent m_i were established for each force component for each step. Its identification was based on a least square procedure between the theoretical and measured values. The identified coefficients are illustrated in Table 2.

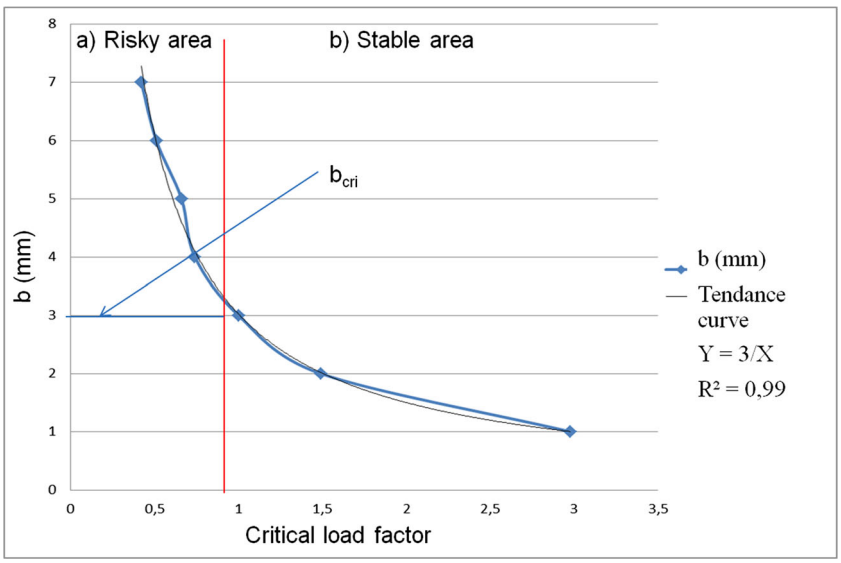

Fig. 9 Stability analysis for a multistep tool

4 Industrial application

4.1 Stability analysis

In this section, the presented model is applied in order to evaluate the stability of a boring multistep tool operation. This model uses the FRF matrix at the tool extremity and the cutting laws based on the Kienzle model. The corresponding parameters for two major tool cutting edge (85° and 90°) are given in Table 2.

Figure 8 shows stability diagrams for the multistep tool for a given depth of cut of the last step b^{E_3}. Because of the casting process, this maximal depth of cut for the last step goes up to 5 mm (Fig. 1). Knowing that Fig. 8c is drawn for $b^{E_3} = 3$ mm, it shows that the horizontal line passing by η=1 is tangent to the minimal points of the lobes. This means that $b^{E_3} = 3$ mm is the critical depth of cut b_{cri}. Figure 8d shows that for $b^{E_3} = 4$ mm $(4\text{ mm} > b_{cri})$ and $N = 750$ RPM, the horizontal line for η=1 is situated in the stable domain.

Figure 8a, b indicates that the operation is always stable. For $b^{E_3} = 1$ mm and $b^{E_3} = 2$ mm. Indeed, the lobes are everywhere above η=1.

The critical load factor η_{cri} is defined as the load factor corresponding to the horizontal line tangent to the lobes as shown in Fig. 8a.

4.2 Stability tolerance analysis

For a better understanding of the width of cut influence on stability, many simulations allow the elaboration of a diagram representing the simulated depth of cut and the critical load factor. Figure 9 represents two main domains separated by a red vertical line. The stable domain corresponds to a load factor greater than 1. When the load factor is lower than 1, there is a risk of instability; however ,some cutting conditions may be stable if the revolution speed is well selected (Fig. 8d).

It is important to remind that the critical width of cut correspond to η=1. Therefore, having this diagram, the security limits can be controlled and operation better designed.

5 Conclusion

In this paper we have proposed and tested a stability approach for a multistep tool for the boring process. The use of the force mechanical screw at the tool tip allows the establishment of the boring process equation. This one, solved in the frequency domain, allows the stability state evaluation, through a drawing of the load factor evolution. In order to get the FRF matrix at the tool tip, we have used the receptance coupling method mixing experimental data and numerical data coming from a finite element model of the tool.

The application of this stability approach on an industrial case has shown the stability limits for the studied operation and can contribute to enhance tool design. However, this model can be applied only on tools having a constant pitch. The use of a variable pitch tool makes the solving of the characteristic equation of the boring process very complex in the frequency domain. This is why a resolution in the time domain can make the presented method general for all multistep tools.

References

1. Peklenik J, Gartner J (1967) Workpiece accuracy criterion for the dynamic machine tool acceptance test. Int J Mach Tools Des Res 7(4):303–324
2. Pruvot F (1995) Conception et calcul des machines-outil. Benstone Instrum 3:344
3. Koppka F (2008) A contribution to the maximization of productivity and workpiece quality of the reaming process by analyzing its static and dynamic behavior: an analysis with focus on automative powertrain production. PhD thesis, Darmstadt technical university
4. Hai Long W, Research on lathe flutter analysis and suppression method (2013) Mechanical manufacturing and automation
5. Tlusty J, et Spacek L (1954) Self-excited vibrations on machine tools. Publication of the Czech Academy of Sciences (Nakl. CSAV in Czech)
6. Tobias S (1965) Machine tool vibration. Blackies and Son, London
7. Altintas Y, Budak E (1995) Analytical prediction of stability lobes in milling. CIRP Ann Manuf Technol 44:357–362
8. Altintas Y, Engin S, Budak E (1999) Analytical stability prediction and design of variable pitch cutter. J Manuf Sci Eng 121(2):173–178
9. Budak E (2000) Improving productivity and part in milling of titanium based impellers by chatter suppression and force control. Ann CIRP 49(1):31–36
10. Altintas Y, Stepan G, Merdol D, Dombovari Z (2008) Chatter stability of milling in frequency and discrete time domain. CIRP J Manuf Sci Technol 1(1):35–44
11. Jochem C, et Altintas Y (2007) Generalized modeling of drilling vibrations. Part ii : chatter stability in frequency domain. Int J Mach Tools Manuf 47(9):1474–1485, **Selected papers from the 2nd International Conference on High Performance Cutting 2nd {CIRP} International Conference on High Performance Cutting**
12. Bayly PV, Metzler SA, Young KA, Halley JE (1999) Analysis and simulation of radial chatter in drilling and reaming. ASME Design Engineering Technical Conference, DETC/VIB8059, Las Vegas, Nevada
13. Roukema JC, Altintas Y (2006) Time domain simulation of torsionalâaxial vibrations in drilling. Int J Mach Tools Manuf 46(15):2073–2085
14. Selmi J, Costes J-P, Lorong P, Poulachon G, Carras P (2014) Prediction of the spindle and tool receptance: industrial application in reaming process. HSM, Prague
15. Erturk A, Ozguven H, Budak E (2006) Analytical modeling of spindle-tool dynamics on machine tools using Timoshenko beam

model and receptance coupling for the prediction of tool point FRF. Int J Mach Tools Manuf 46(15):1901–1912
16. Ozsahin O, Erturk A, Ozguven H, Budak E (2009) A closedform approach for identification of dynamical contact parameters in spindle-holder-tool assemblies. Int J Mach Tools Manuf 49(1):25–35
17. Albertelli P, Goletti M, Monno M (2003) A new receptance coupling substructure analysis methodology to improve chatter free cutting conditions prediction. Int J Mach Tools Manuf 72(16)
18. Kienzle O, Victor H (1957) Spezi_sche shnittkraefte bei der metallbearbeitung. Werkstattstehnik und Maschinenbau 47:322